


# Strengthening Mechanisms on $(\text{Cu}-10\text{Zn})_{100-x-x}$ wt% $\text{Al}_2\text{O}_3$ ( $x = 0, 3, 6, 9$ and $12$ ) Nanocomposites Prepared by Mechanical Alloying and Vacuum Hot Pressing: Influence of Reinforcement Content

S. Sivasankaran<sup>1</sup>  · K. R. Ramkumar<sup>1</sup> · Abdulaziz S. Alaboodi<sup>1</sup>

Received: 9 November 2016 / Accepted: 24 January 2017 / Published online: 10 February 2017  
© The Indian Institute of Metals - IIM 2017

**Abstract** In the present research work, novel  $(\text{Cu}-10\text{Zn})_{100-x-x}$  wt%  $\text{Al}_2\text{O}_3$  ( $x = 0, 3, 6, 9$  and  $12$ ) nanocomposites were manufactured by mechanical alloying process and vacuum hot-pressing technique. As-sintered hot pressed samples exhibited crystallite size of 280, 230, 184, 152 and 122 nm with properties of nano-alumina particles which were examined by transmission electron microscopy. The influence of nano ceramic alumina content in  $\text{Cu}-10\text{Zn}$  nanocrystallite matrix on mechanical behavior was investigated by simple uniaxial compression test. The examination of compressive results revealed that  $(\text{Cu}-10\text{Zn})_{94-6}\text{Al}_2\text{O}_3$  nanocomposite was more work hardening than others. Several strengthening mechanisms, namely, particle strengthening, grain boundary strengthening, solid solution strengthening and dislocation–dislocation interactions were quantitatively estimated and correlated with measured compression strength results. It was found that the grain size and dispersion strengthenings contributed significantly to the total strength.

**Keywords** Cu–Zn alloy · Mechanical alloying · Characterization · Mechanical properties · Strengthening mechanisms

## 1 Introduction

The incorporation of nano-particles and decreasing the crystallite size from micron to nano in the matrix enhances the mechanical properties of metal matrix composites. Improvement in mechanical properties result in changes in hardness, Young's modulus, yield strength, ultimate tensile strength, ductility in terms of work hardening and ultimate compressive strength [1–3]. Now a days, the Cu–Zn alloys, called brass, is a material of considerable research interest, as it has distinctive properties such as strength, ductility, electrical conductivity, corrosion resistance and good machinability. Further, it can be used in several sectors namely automotive industries, construction field, electrical, ammunition and precision industry [4]. Single phase substitutional solid face-centred cubic (FCC) structure of Cu–Zn alloy can be obtained if Zn is less than 35% in the Cu; known as  $\alpha$ -brass. This  $\alpha$ -brass has the average yield strength of 200–300 MPa which mainly depends on processing method. To enhance the mechanical properties of  $\alpha$ -brasses and enhance its applications in wide ranges, it is necessary to modify its grains into nano-structured/ultra-fine level by using severe plastic deformation technique and/or incorporation of second phase nano-particles in the structure [5]. Further, the mechanical and structural properties of copper based alloys can be improved by the addition of nano-alumina, as alumina will enhance these properties extensively when compared to other reinforcements [6].

In general, Cu based metal matrix composites can be manufactured via solid state and or liquid state method. However, wettability, homogeneous distribution and embedding of second phase particles in the Cu matrix are the major issues in liquid state consolidation technique. It can be avoided in solid state consolidation technique and

✉ S. Sivasankaran  
sivasankarangs1979@gmail.com

K. R. Ramkumar  
get2raam@gmail.com

Abdulaziz S. Alaboodi  
alaboodi@qec.edu.sa

<sup>1</sup> Department of Mechanical Engineering, College of Engineering, Qassim University, Buraydah, Kingdom of Saudi Arabia

moreover, nano-structured and nano-reinforcement can be easily achieved. In addition, the synthesis of nanocomposites via casting, conventional powder metallurgy and extrusion are very difficult due to clustering of nano-particles. It can be completely eliminated by solid state mechanical alloying which is one of the severe plastic deformation technique involving repeated plastic deformation, welding and fracturing of matrix particles inside the high-energy ball mill [7–9]. Mechanical alloying followed by vacuum hot pressing is the best consolidation method and also economical one by which the formation of nanostructure by grain refinement and embedding of nano-particles is possible [10]. The improvement of mechanical properties by decreasing the grain size from matrix and effective embedding of nano-reinforcements are possible by mechanical alloying [11]. Vacuum hot pressing is based on low strain rate powder consolidation at elevated temperature and is cost-effective when compared to hot isostatic pressing [12]. In hot pressing, both heating and pressing are applied so that improvement in powder particles' contact, sufficient atomic diffusion and high densification can be possible [13].

Achievement of improved mechanical strength via MA is due to the contribution of various strengthening mechanisms namely grain size, solid solution, dislocation and dispersion strengthening [14]. Therefore, the reduction of crystallite size in  $\alpha$ -brass from micron into ultra-fine/nano level, incorporation of nano-alumina particles, variation in dislocations and solid solution of Zn by SPD of MA are important to express the contribution of various strengthening mechanisms on improvement in mechanical strength quantitatively [15, 16]. There is no research work to address these details for the scientific community. Already, our research groups have published the synthesis and characterization of Cu–Zn matrix reinforced with nano-alumina by MA [17]. Therefore, the present study has been designed into three objectives: first, consolidate the nanostructured/nanocomposite powders of (Cu–10Zn)-Al<sub>2</sub>O<sub>3</sub> into bulk sample via vacuum hot pressing; second, to characterize all microstructural features by transmission electron microscopy (TEM), investigate the mechanical behavior in terms of ultimate compressive strength, work hardening rate by simple compression test; and third, quantify the contribution of each strengthening mechanisms on total strength by developing various models.

## 2 Experimental Procedure

### 2.1 Materials Processing

The initial raw materials of copper (Cu) and zinc (Zn) powders (99.4% purity, average particle size of less than

45  $\mu\text{m}$ ) were purchased from Lobachemi, India which were used as matrix materials. The purchased nano-alumina (Al<sub>2</sub>O<sub>3</sub>) had more than 99% purity and an average particle size of 80 nm. The nano-composites of six samples of (Cu–10Zn)<sub>100-x-x</sub> wt.Al<sub>2</sub>O<sub>3</sub> ( $x = 0, 3, 6, 9$  and  $12$  wt%) were synthesized by high-energy mechanical alloying. The as-received elemental powders were put into two station planetary ball mill with ball milling parameters of 10:1 ball-to-powder ratio, 20 h milling time and 280 rpm mill speed. The mechanical alloying processes were carried out under wet milling method (toluene). The detailed synthesis procedure was explained elsewhere [17]. The manufactured nanocomposite powders were compacted using uniaxial compaction die of 600 MPa using high carbon high chromium D3 tools steel of 10 mm diameter. Then, the samples were sintered at 900 °C under vacuum of  $10^{-3}$  torr with 25 MPa constant uniaxial pressure for 1 h. During vacuum hot pressing, graphite die was used. After vacuum hot pressing, the sample was cooled to room temperature in the vacuum hot pressing furnace itself.

### 2.2 Materials Characterization

The Archimedes' principle was used to measure the density of sintered bulk samples. Based on weight fraction (i.e. rule of mixture) and density of each constituent, the theoretical densities were calculated. The density of copper (Cu), zinc (Zn) and aluminium oxide (Al<sub>2</sub>O<sub>3</sub>) were 8.96 g/cm<sup>3</sup>, 7.13 g/cm<sup>3</sup> and 3.95 g/cm<sup>3</sup> respectively. The following formula was used to estimate the densities of sintered samples.

$$\rho_s = \frac{W_{air}}{(W_{air} - W_{sus})} \times \rho_w, \quad \text{g/cm}^3 \quad (1)$$

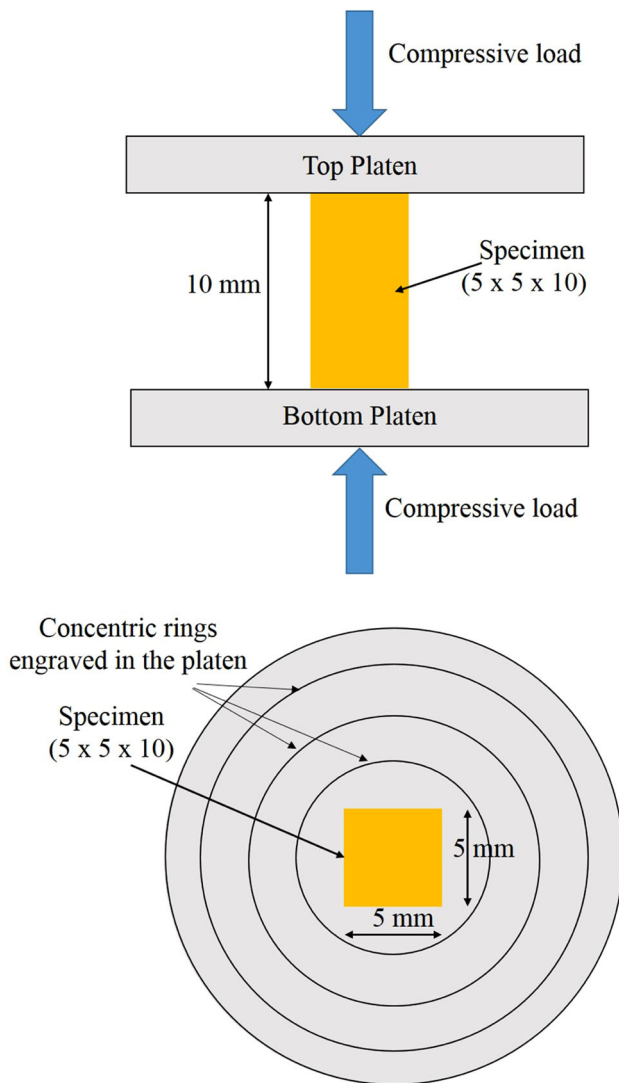
where  $W_{air}$  is the weight of the sintered sample in air column,  $W_{sus}$  is the weight of the sintered sample suspended in water column,  $\rho_w$  is the density of water (1 g/cm<sup>3</sup>). The sample chemical composition, sintered bulk density and its relative density is shown in Table 1. To characterize the solid sintered samples, manual polishing and Ion milling were done until the thickness was around 100 nm. Then, the samples as thin nano-foil were dimpled for transmission electron microscope (TEM) characterization. The fabricated bulk sintered nano-composite samples were then characterized using transmission electron microscopy (TEM, JEOL JEM 2100) by bright field images and selective area diffraction pattern (SADP).

### 2.3 Compression Test

Compression test samples with sizes of  $5 \times 5 \times 10$  mm were prepared using wire cut electric discharge machining from bulk sintered samples. After wire cut, the samples

**Table 1** The sample chemical composition, bulk density and its relative density of (Cu–10Zn)<sub>100-x-x</sub> wt% Al<sub>2</sub>O<sub>3</sub> nanocomposites

Sample	Zn content (wt %)	Weight % of Al <sub>2</sub> O <sub>3</sub>	Theoretical density (g/cm <sup>3</sup> )	Bulk density (g/cm <sup>3</sup> )	Relative density (%)
Cu–10Zn–0Al <sub>2</sub> O <sub>3</sub>	10	0	8.77	8.38 ± 0.04	95.55
Cu–10Zn–3Al <sub>2</sub> O <sub>3</sub>	10	3	8.62	8.15 ± 0.02	94.54
Cu–10Zn–6Al <sub>2</sub> O <sub>3</sub>	10	6	8.48	7.95 ± 0.01	93.75
Cu–10Zn–9Al <sub>2</sub> O <sub>3</sub>	10	9	8.33	7.75 ± 0.03	93.03
Cu–10Zn–12Al <sub>2</sub> O <sub>3</sub>	10	12	8.19	7.45 ± 0.02	90.96

**Fig. 1** The sample size and its position in compression platens for simple compression test

were polished using silicon carbide (SiC) emery sheets. The prepared sample size and its shape for simple compression test is shown in Fig. 1. As shown in Fig. 1, the height of sample of 10 mm with a square cross section of 5x5 mm was used as per ASTM E9 standard. The uni-axial

compression test was carried out using servo controlled universal testing machine with a strain rate of  $10^{-4} \text{ s}^{-1}$  at room temperature. The fracture surface after compression test was also examined using scanning electron microscope (SEM, JEOL JSM 6390) to investigate the fracture mechanisms. The compressive mechanical properties investigated here was based on averages of three samples.

### 3 Results and Discussion

#### 3.1 Examination on Bulk Sintered Density

The theoretical density of fabricated samples have been estimated using rule of mixture and the bulk density has been measured according to Archimedes principles (Table 1). From Table 1, it is observed that the bulk sintered density starts to decrease slightly as function of reinforcement of Al<sub>2</sub>O<sub>3</sub> on Cu–10Zn nanocrystallite matrix. This may be attributed to more strain hardening obtained from mechanical alloying process for the same mechanical alloying time of 20 h. The 12 wt% Al<sub>2</sub>O<sub>3</sub> reinforced Cu–10Zn nano-crystallite matrix is the more strain hardened one when compared to un-reinforced Cu–10Zn nanocrystallite matrix as alumina acts as milling agent in addition to other milling media such as milling speed, ball-to-powder ratio and milling time. In addition, the hard-reinforcing particles of nano-alumina is expected to impede/hinder the plastic deformation of Cu–10Zn nanocrystallite matrix during consolidation, which ultimately decreases the diffusion process. Further, the slight decreased density value as a function of nano-reinforcement is expected to increase the dispersion strengthening due to increase in the amount of nano-alumina particles, dislocation strengthening due to refinement in the matrix and grain size strengthening of Cu–10Zn matrix due to decrease in matrix crystallite size with increase in the amount of alumina. Moreover, the density of nano-alumina was lower than the Cu–10Zn matrix. Therefore, full densification on particle reinforced metal matrix nanocomposite powder is difficult to achieve. However, in the

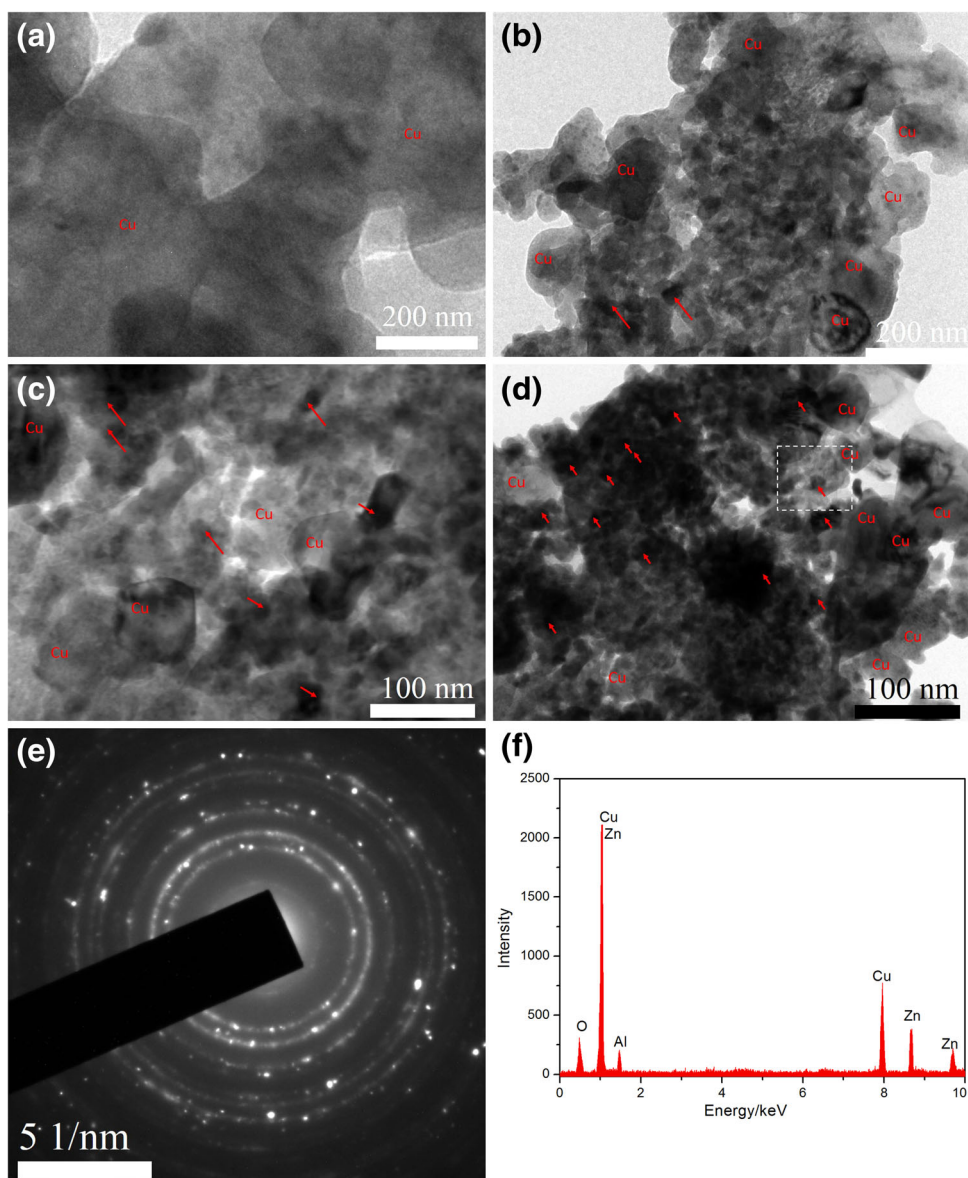
present investigation, all the samples have relative density of more than 90%.

### 3.2 TEM Microstructure

The x-ray diffraction (XRD) analysis and powder surface morphology examination on  $(\text{Cu-10Zn})_{100-x-x}$  wt%  $\text{Al}_2\text{O}_3$  nanocomposites have been explained in our previous work [17]. After mechanical alloying, the Cu–10Zn matrix powder crystallite sizes are 77 nm, 55 nm, 42 nm, 30 nm and 25 nm for 0, 3, 6, 9 and 12 wt% reinforced nano- $\text{Al}_2\text{O}_3$  respectively, which have been conformed by TEM of powder samples [17]. XRD, SEM morphology on milled powders and TEM results explains the successful fabrication of the present nanocomposite powder under steady

state condition [17]. Figure 2a–d show the TEM micrograph of Cu–10Zn,  $(\text{Cu-10Zn})_{94-6}\text{Al}_2\text{O}_3$ ,  $(\text{Cu-10Zn})_{91-9}\text{Al}_2\text{O}_3$  and  $(\text{Cu-10Zn})_{88-12}\text{Al}_2\text{O}_3$  nanocomposites respectively. The observed sintered Cu–10Zn matrix crystallite sizes are  $280 \pm 14$ ,  $184 \pm 8$ ,  $152 \pm 11$  and  $122 \pm 6$  nm for 0, 6, 9 and 12 wt% nano-alumina reinforced nanocomposites respectively. These sintered matrix crystallite sizes are calculated based on several bright field images (Fig. 2). In each sample, around 250 crystallites have been counted and averaged for investigation. It is observed that the Cu–10Zn matrix crystallite size increases considerably after sintering due to crystal growth. However, all the sintered samples have the crystallite size under ultra-fine level in which around 80 nm of nano-alumina are embedded in the Cu–10Zn matrix. Moreover, the crystal

**Fig. 2** TEM bright field images of Cu–Zn nanocrystallite matrix reinforced with nano  $\text{Al}_2\text{O}_3$ : **a** 0%  $\text{Al}_2\text{O}_3$ ; **b** 6%  $\text{Al}_2\text{O}_3$ ; **c** 9%  $\text{Al}_2\text{O}_3$ ; **d** 12%  $\text{Al}_2\text{O}_3$ ; **e** SAED patterns on **(d)**; **f** Corresponding EDS on **(d)**. The red arrows indicate the nano-alumina phases in Cu–Zn matrix phases



growth decreases as a function of dispersoid refinement, due to dislocation pinning effect between nano-alumina and Cu–10Zn matrix. Figure 2e shows the corresponding selective area diffraction (SAD) pattern on (Cu–10Zn)<sub>88</sub>–12Al<sub>2</sub>O<sub>3</sub> sample in which continuous ring patterns are observed indicating that the fabricated composite is under nano/ultrafine level. The energy dispersive spectrum analysis is also done on (Cu–10Zn)<sub>88</sub>–12Al<sub>2</sub>O<sub>3</sub> TEM sample in which the presence of nano-alumina, Cu–Zn matrix phases have been confirmed. It is observed from XRD results that there is no Zn peak phase after mechanical alloying (20 h) due to solid solution of Zn solute atoms on Cu solvent atoms. However, Fig. 2f of EDS results shows the presence of Zn phase in the sample. Therefore, based on XRD and TEM EDS results, it can be confirmed that the solid solution of Zn on Cu matrix phase had occurred. In addition, the nano-alumina particles are represented in solid red color arrow in which some nano-alumina particles are embedded on Cu–10Zn matrix phases and some nano-alumina particles are on Cu–10Zn matrix grain boundary. Especially, for higher-reinforced sample (Fig. 2d, it is shown that there are more and more nano-alumina particles embedded on the matrix and are located in the matrix grain boundary. A similar behavior has also been observed by Liu et al. [18]. The dispersed nano-alumina particles in the matrix phases are expected to increase the strength of matrix which has also been reported by Zhao et al. [19]. The located nano-alumina on matrix grain interface or boundary can enhance the resistance to cracking which ultimately improves the ductility or strain hardening. Further, these intragranular nano-alumina particles can impede/pin down the matrix crystallites and accumulate the dislocations in the matrix crystallites. Hence, the nano-alumina is expected to serve for improving the mechanical strength and work hardening.

It is well known that the crystal size will depend on both nucleation rate and its growth rate. Since, in the present work, the samples are under solid phase, crystal size mainly depends on growth rate with respect to sintering temperature and percentage of nano-alumina particles. However, the second phase nano-alumina particles will promote the heterogeneous nucleation. This mean, when the particles have poor contact angle (wetting angle), nucleation is encouraged [20]. Increasing nano-alumina particles in the matrix can enhance number of nuclei and hence the crystal sizes are refined as a function of reinforcement. Further, the dispersed nano-alumina as second phase particles can prevent the movement of crystallite during sintering, which mean hindering the crystal growth. This can be due to more Zener pinning pressure. This Zener pinning pressure can increase as a function of second phase particles as mentioned the in Eq. (2) [21]:

$$P_z = \frac{3F_v\gamma}{t} \quad (2)$$

where  $P_z$  is Zener pinning pressure,  $F_v$  is the volume fraction of second phase particles,  $\gamma$  is the grain boundary energy per unit area and  $t$  is the average crystallite size. As per the Eq. (2), the Zener pinning pressure starts to increase by the addition of second phase particles of nano-alumina in the Cu–10Zn matrix. Therefore, the interfacial bond between nano-alumina and Cu–Zn matrix, and amount of second phase nano-alumina particles in the matrix can define the mechanical strength and ductility of the present nanocomposites.

### 3.3 Compressive Stress–Strain Curves

Figure 3 and Table 2 show the compressive engineering stress–strain curves for (Cu–10Zn)<sub>100–x–x</sub> wt% Al<sub>2</sub>O<sub>3</sub> nanocomposites ( $x = 0, 3, 6, 9$  and  $12$ ). The ultimate compressive strength (UCS) of Cu–10Zn, (Cu–10Zn)<sub>97</sub>–3Al<sub>2</sub>O<sub>3</sub>, (Cu–10Zn)<sub>94</sub>–6Al<sub>2</sub>O<sub>3</sub>, (Cu–10Zn)<sub>91</sub>–9Al<sub>2</sub>O<sub>3</sub> and (Cu–10Zn)<sub>88</sub>–12Al<sub>2</sub>O<sub>3</sub> are 380 MPa, 420 MPa, 810 MPa, 840 MPa and 890 MPa respectively. It is clear that the UCS of Cu–10Zn is much lower when compared to (Cu–10Zn)<sub>88</sub>–12Al<sub>2</sub>O<sub>3</sub> sample; which is around 2.34 times lower. However, the compression of Cu–10Zn sample exhibits 18.2% strain-to-failure which is around 58% more than (Cu–10Zn)<sub>88</sub>–12Al<sub>2</sub>O<sub>3</sub> sample. The increased UCS with function of nano-alumina is expected to contribute to crystallite size reduction, dispersion strengthening and dislocation strengthening (Fig. 2). The fabricated nanocomposites of (Cu–10Zn)<sub>94</sub>–6 wt% Al<sub>2</sub>O<sub>3</sub>, (Cu–10Zn)<sub>91</sub>–9 wt% Al<sub>2</sub>O<sub>3</sub> and (Cu–10Zn)<sub>88</sub>–12 wt% Al<sub>2</sub>O<sub>3</sub> have highest UCS when compared to the work done by previous authors (Kang et al. [22] achieved 455 MPa in Cu–10% CNT and 581 MPa in Cu–15% CNT metal matrix

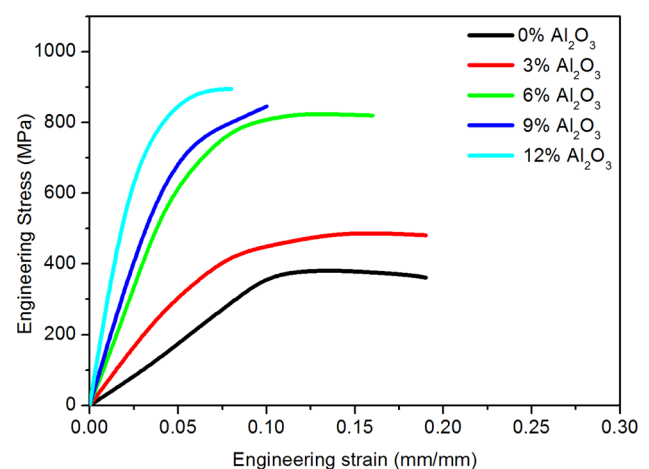


**Fig. 3** Compressive engineering stress–strain curves of (Cu–10Zn)<sub>100–x–x</sub> wt% Al<sub>2</sub>O<sub>3</sub> ( $x = 0, 3, 6, 9$  and  $12$ ) nanocomposites

**Table 2** The crystallite size, dislocation density and compressive properties of (Cu–10Zn)<sub>100-x-x</sub> wt% Al<sub>2</sub>O<sub>3</sub> sintered nanocomposites

Sample	Volume fraction of fibre (V <sub>f</sub> )	Crystallite size (t), nm	Dislocation density (ρ), × 10 <sup>14</sup> m <sup>-2</sup>	RMS strain <ε <sub>rms</sub> >	Lattice parameter (a), nm	UCS (MPa)	Compressive strain-to-failure (%)	Strain hardening exponent (n)
Cu–10Zn–0Al <sub>2</sub> O <sub>3</sub>	0.0000	280 ± 15	0.8348	0.08365	0.3506	380	18.2	0.65
Cu–10Zn–3Al <sub>2</sub> O <sub>3</sub>	0.0229	230 ± 10	1.0123	0.08483	0.3569	425	16.3	0.42
Cu–10Zn–6Al <sub>2</sub> O <sub>3</sub>	0.0462	184 ± 12	1.4251	0.08679	0.3243	810	14.5	0.34
Cu–10Zn–9Al <sub>2</sub> O <sub>3</sub>	0.0699	152 ± 08	2.0156	0.08702	0.2783	840	12.0	0.41
Cu–10Zn–12Al <sub>2</sub> O <sub>3</sub>	0.0939	122 ± 11	2.4934	0.08732	0.2812	890	11.5	0.55

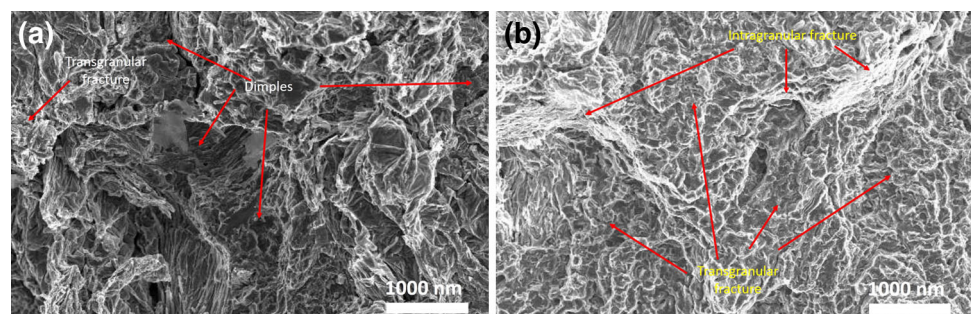
nanocomposite, Cha et al. [23] achieved 448 MPa in Cu–23% CNT nanocomposites). Among the samples, the UCS starts to increase steadily from 420 MPa to 810 MPa between (Cu–10Zn)<sub>97–3</sub>Al<sub>2</sub>O<sub>3</sub> and (Cu–10Zn)<sub>94–6</sub>Al<sub>2</sub>O<sub>3</sub> samples. These results are expected to form a good interfacial bonding between second phase nano-alumina particles and Cu–10Zn matrix (Fig. 2); hence, the load is transferred effectively from the matrix to second phase particles in (Cu–10Zn)<sub>94–6</sub>Al<sub>2</sub>O<sub>3</sub> sample. However, beyond 6% Al<sub>2</sub>O<sub>3</sub>, though the UCS started to increase, it was improved slightly. These results indicate that the decreased increment in UCS as a function of nano-alumina beyond 6% Al<sub>2</sub>O<sub>3</sub> can be attributed to decrease in the interfacial bonding. Therefore, the present investigation works up to the addition 12% Al<sub>2</sub>O<sub>3</sub>. To establish and examine the mode of fracture in the present developed nanocomposites, fractography is also studied based on fractured SEM images of (Cu–10Zn)<sub>97–3</sub> wt% Al<sub>2</sub>O<sub>3</sub> nanocomposite and (Cu–10Zn)<sub>88–12</sub> wt% Al<sub>2</sub>O<sub>3</sub> nanocomposites which is shown in Fig. 4. In general, ductile fracture can be characterized by a dimple structure whereas the brittle fracture can be characterized by both intergranular and transgranular fracture. From Fig. 4a, it is clear that large and more dimple fracture has occurred in 3 wt% Al<sub>2</sub>O<sub>3</sub> reinforced nanocomposite which indicates considerable ductility possessed by the material. Thus

Fig. 4a explains that ductile dimple fracture mechanism is due to void nucleation, growth and coalescences. It is expected here that the voids can be developed at nanocrystallite matrix grain boundaries and at the interface of ceramic alumina particle and matrix. These voids can form sub-micron level dimples, consequently joining of voids and finally spreading of cracks. However, large amount of intergranular brittle fractures and transgranular brittle fractures are formed in (Cu–10Zn)<sub>88–12</sub> wt% Al<sub>2</sub>O<sub>3</sub> nanocomposite (Fig. 4b). These results are expected to be responsible for more sites of nucleation of dimples which in turn arises from increased interface area between ceramic particles and matrix. As a result, the ultimate compressive strength at room temperature shifts to high value in the case of (Cu–10Zn)<sub>88–12</sub> wt% Al<sub>2</sub>O<sub>3</sub> nanocomposite when compared to (Cu–10Zn)<sub>97–3</sub> wt% Al<sub>2</sub>O<sub>3</sub> nanocomposite.

### 3.4 Examination of Ductility

The ductility of any metals/alloys/composites usually express in terms of work hardening/strain hardening/cold workability by plastic deformation. Further, the strengthening usually occurs due to dislocation movements and dislocation generation in the crystal [24].

**Fig. 4** Fractography SEM images of compressed samples of: **a** (Cu–10Zn)<sub>97–3</sub> wt% Al<sub>2</sub>O<sub>3</sub> nanocomposites **(b)** (Cu–10Zn)<sub>88–12</sub> wt% Al<sub>2</sub>O<sub>3</sub> nanocomposites



The work hardening rate can be calculated by the following expression.

$$\Theta = \frac{d\sigma_T}{d\varepsilon_T} \tag{3}$$

where  $\Theta$  is work hardening rate,  $d\sigma_T$  is the difference/changes in true stress of consecutive values,  $d\varepsilon_T$  is the difference/changes in true strain of consecutive values. It is well known that good uniform elongation can be obtained from metals when the metals has high work hardening rate as it helps to delay the localized deformation called necking during load [19]. The variation of work hardening rate against true strain for the present nanocomposite is shown in Fig. 5. As shown in Fig. 5, the nanocomposite of  $(\text{Cu-10Zn})_{94-6}\text{Al}_2\text{O}_3$  exhibit more work hardening rate when compared to all other samples investigated here. This is expected to attain good interfacial bonding between nano-alumina and Cu-10Zn matrix, more ordered dislocation accumulation and obstruction in-and-around nano-alumina particles and grain boundaries over the matrix. Further, the nanocomposites of Cu-10Zn,  $(\text{Cu-10Zn})_{97-3}\text{Al}_2\text{O}_3$  show considerable work hardening rates lower than  $(\text{Cu-10Zn})_{94-6}\text{Al}_2\text{O}_3$  nanocomposite. These results show lower amount of dislocations in the structure. However,  $(\text{Cu-10Zn})_{91-9}$  wt%  $\text{Al}_2\text{O}_3$  and  $(\text{Cu-10Zn})_{88-12}$  wt%  $\text{Al}_2\text{O}_3$  nanocomposites exhibit poor work hardening. This is expected to lead to improper bonding or decreased wettability between nano-alumina particles in the Cu-Zn matrix due to more volume of nano-alumina particles. Therefore, based on the results of work hardening rate, the optimum and best sample is  $(\text{Cu-10Zn})_{94-6}\text{Al}_2\text{O}_3$ , which can be selected for structural applications and others. Double logarithmic curves on true stress-true strain of  $(\text{Cu-10Zn})_{100-x-x}$  wt%  $\text{Al}_2\text{O}_3$  nanocomposites ( $x = 0, 3, 6, 9$  and 12) during work hardening period is shown in Fig. 6.

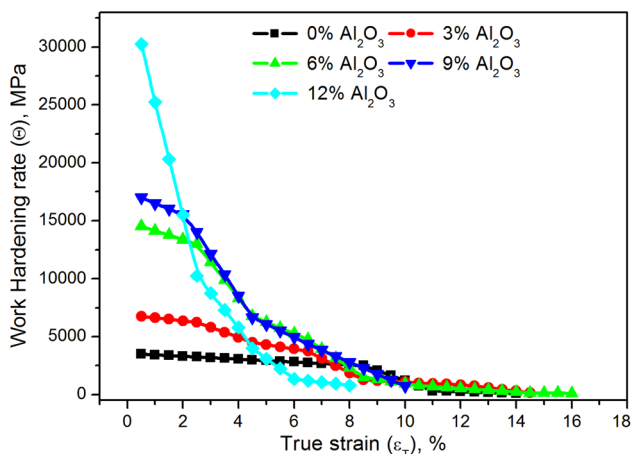


**Fig. 5** The variation of work hardening rate against true strain of  $(\text{Cu-10Zn})_{100-x-x}$  wt%  $\text{Al}_2\text{O}_3$ , ( $x = 0, 3, 6, 9$  and 12)

The Hollomon equation has been used to determine the strain hardening exponent ( $n$ ) and the equation is given below:

$$\sigma_T = K\varepsilon_T^n \tag{4}$$

where  $K$  is a constant,  $\sigma_T$  is true stress,  $\varepsilon_T$  is true strain and  $n$  is the strain hardening exponent. The calculated strain hardening exponents are 0.65, 0.42, 0.34, 0.41 and 0.55 for Cu-10Zn,  $(\text{Cu-10Zn})_{97-3}\text{Al}_2\text{O}_3$ ,  $(\text{Cu-10Zn})_{94-6}\text{Al}_2\text{O}_3$ ,  $(\text{Cu-10Zn})_{91-9}\text{Al}_2\text{O}_3$  and  $(\text{Cu-10Zn})_{88-12}\text{Al}_2\text{O}_3$  respectively. The values of strain hardening exponent for metals usually lies between 0.2 and 0.6 in which the lower value indicates more plastic deformation and higher value indicates more elastic deformation. The conventional copper and its alloy possesses the  $n$  value between 0.35 and 0.40 [25]. Among the samples investigated here, the nanocomposites of  $(\text{Cu-10Zn})_{94-6}\text{Al}_2\text{O}_3$  only exhibit the value of 0.34 which is just nearer to the conventional Cu based alloy. This result indicates that the sample of  $(\text{Cu-10Zn})_{94-6}\text{Al}_2\text{O}_3$  nanocomposite is more work hardening (Fig. 6) when compared to other samples. The other samples exhibit more differences in strain hardening exponent value compared to the conventional one. This large difference in values of other samples may be attributed to the improper/poor interfacial bonding, poor wettability and more dislocation accumulations between nano-alumina particles and matrix phases. Therefore, the other samples may exhibit early particle fracture due to weak interfacial bond and more flaws in the structure. However, the exhibited good work hardening rate for  $(\text{Cu-10Zn})_{94-6}\text{Al}_2\text{O}_3$  nanocomposite can be attributed to strong interfacial bond and proper embedding of nano-alumina in the matrix.

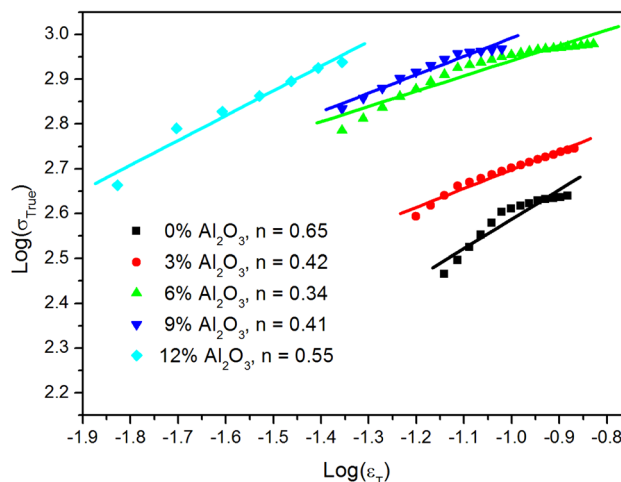


**Fig. 6** Logarithmic curves of true stress–true strain on work hardening rate and linearly fitted curves for  $(\text{Cu-10Zn})_{100-x-x}$  wt%  $\text{Al}_2\text{O}_3$ , ( $x = 0, 3, 6, 9$  and 12) nanocomposites

### 3.5 Evaluation of Various Strengthening Mechanisms

The mechanical properties of metals/alloys/composites can be enhanced by varying the crystallite size/fine grain strengthening, solid solution of minor solute elements over the major solvent element, dislocation/strain hardening and dispersion strengthening by incorporating the reinforcements in the structure. The contribution of various strengthening mechanisms on total strength have been estimated by several models. The various parameters used for estimating various strengthening mechanisms is given in Table 3 and its contribution on total mechanical strength of (Cu–10Zn)<sub>100-x-x</sub> wt% Al<sub>2</sub>O<sub>3</sub> nanocomposites (x = 0, 3, 6, 9 and 12) is also given in Table 4. In the present investigation, the added minor element of Zn is dissolved in the major Cu matrix after mechanical alloying which is confirmed by XRD and EDS results. Due to solid solution of Zn on Cu matrix, the strength of nanocomposites is expected to increase. As per Dixit et al., [26], the contribution of solid solution strengthening increment due to solute atom of Zn is determined as:

$$\Delta\sigma_{ss} = AC_o^{2/3} \tag{5}$$

where, A is the constant and C<sub>o</sub> is the concentration of the solute atom in weight percent. The value of A for zinc (Zn) is 12.431 [26]. Based on Eq. (5), the calculated solid solution strengthening are 57.69 MPa, 56.53 MPa, 55.36 MPa, 54.18 MPa and 52.98 MPa for Cu–10Zn, (Cu–10Zn)<sub>97-3</sub>Al<sub>2</sub>O<sub>3</sub>, (Cu–10Zn)<sub>94-6</sub>Al<sub>2</sub>O<sub>3</sub>, (Cu–10Zn)<sub>91-9</sub>Al<sub>2</sub>O<sub>3</sub> and (Cu–10Zn)<sub>88-12</sub>Al<sub>2</sub>O<sub>3</sub> respectively (Table 4). It can be

**Table 3** Various parameters used for calculating strengthening mechanisms

Parameters	Values	Unit
A value for Zn	12.431	MPa
k	0.14	MPa.m <sup>1/2</sup>
σ <sub>0</sub>	20	MPa
α	0.3	–
M	3	–
G	45000	MPa

observed here that the amount of solid solution strength starts to decrease as a function of reinforcement due to the addition of nano-alumina particles in the matrix. It is well known that fine crystallite/nanocrystallite materials can have higher number of grain boundaries and hence these grain boundaries can impede/hinder the dislocation motion. According to Hall–Petch relation, the contribution of grain boundary strengthening can be estimated as:

$$\sigma_{gs} = \sigma_0 + kt^{-1/2} \tag{6}$$

where t is the crystallite size of the matrix, and σ<sub>0</sub> = 20 MPa and k = 140 MPa μm<sup>1/2</sup> for pure Cu (Li et al. 2015 [27]). It is observed from Table 4 that the strength due to matrix crystallite size variation starts to increase from 284 MPa to 420 MPa considerably as a function of nano-alumina particles in the matrix.

The dislocations, which are majorly responsible for work hardening, are usually accumulated in the form of stress fields on the grain boundaries. The presence of these stress fields can hinder the dislocation motion by repulsive and or attractive interactions [28]. The dislocation density is directly proportional to yield strength of materials. The contribution of strength by dislocation can be estimated by:

$$\sigma_{dis} = \alpha M G b \rho^{1/2} \tag{7}$$

where α is a constant of the order of 0.3, M is the Taylor factor (M = 3 for FCC material), ρ is the dislocation density [29] and can be determined from XRD analysis [6], b is the burgers vector of dislocation in m which is equal to a/√2 for the FCC structure, a is lattice parameter in m [14] and G is shear modulus which is 45 GPa. The dislocation density can be calculated from Eq. (8) as shown below:

$$\rho = 2\sqrt{3} \frac{\langle \epsilon_{r.m.s} \rangle}{tb} \tag{8}$$

where <ε<sub>r.m.s</sub>> is RMS lattice strain which can be determined as:

$$\langle \epsilon_{r.m.s} \rangle = \left( \frac{2}{\pi} \right)^{1/2} \left( \frac{\Delta d}{d_{0(hkl)}} \right) \tag{9}$$

Δd = d<sub>(hkl)</sub> – d<sub>0(hkl)</sub>, where d<sub>(hkl)</sub> is the calculated interplanar spacing, d<sub>0(hkl)</sub> is the observed interplanar spacing.

**Table 4** The contribution of various strengthening mechanisms on mechanical strength of (Cu–10Zn)<sub>100-x-x</sub> wt% Al<sub>2</sub>O<sub>3</sub> nanocomposites

Sample	Solid solution (σ <sub>ss</sub> ) MPa	Hall–Petch (σ <sub>gs</sub> ) MPa	Dislocation (σ <sub>dis</sub> ) MPa	Orowan (σ <sub>disper</sub> ) MPa	Total predicted strength (σ <sub>Total</sub> ) MPa	Actual UCS MPa
Cu–10Zn–0Al <sub>2</sub> O <sub>3</sub>	57.70	284.57	94.71	–	436.98	380
Cu–10Zn–3Al <sub>2</sub> O <sub>3</sub>	56.54	311.92	104.3	106.26	579.01	425
Cu–10Zn–6Al <sub>2</sub> O <sub>3</sub>	55.36	334.37	123.77	175.01	688.51	810
Cu–10Zn–9Al <sub>2</sub> O <sub>3</sub>	54.18	379.09	147.19	243.66	824.12	840
Cu–10Zn–12Al <sub>2</sub> O <sub>3</sub>	52.98	420.81	163.71	316.36	953.86	890



It is observed from Table 4 that the contribution of strengthening by dislocation starts to increase as a function of nano-alumina particles due to more accumulation of dislocations/defects in the structure engendered by high-energy mechanical alloying process and/or severe plastic deformation. The mechanical strength of metals/alloys/composites can be enhanced by incorporating insoluble second phase fine particles (here nano-alumina hard ceramic particles), its homogeneous distribution and its embedded nature in the matrix phase. The dislocation motion of matrix can be delayed/affected by the second phase particles which eventually vary the mechanical properties. The contribution of Orowan strengthening due to the addition of nano-alumina particles is determined by Hsu et al. 2006 [30]:

$$\sigma_{disper} = \frac{0.81Mgb}{2\pi(1-\nu)^{1/2}\lambda} \ln \left[ 2\sqrt{\frac{2}{3}} \frac{r}{r_0} \right] \quad (10)$$

where,  $\nu$  ( $\approx 0.34$ ) is Poisson’s ratio,  $r_0$  ( $\approx 4b$ ) is the dislocation core radius. From Table 4, it is clear that the contribution of dispersion strengthening significantly increases as a function of nano-alumina particles in the matrix. Based on linear superposition, the total strength is determined using the following expression:

$$\sigma_{tot} = \sigma_{ss} + \sigma_{gs} + \sigma_{dis} + \sigma_{disper} \quad (11)$$

From Table 4, it is obvious that the contribution of grain size strengthening on total strength is more for all the samples followed by dispersion strengthening, dislocation strengthening and solid solution strengthening. The measured total ultimate compressive strength is deviated. This may be attributed to unchanged Hall–Petch coefficient due to the presence of nano-alumina in the matrix and uncontrollable factors. The contribution of various strengthening mechanisms on total strength for (Cu–10Zn)<sub>88</sub>–12Al<sub>2</sub>O<sub>3</sub> nanocomposite as an example is shown in Fig. 7. It is very clear that the contributed solid solution, grain size strengthening, dislocation strengthening and dispersion strengthening are 5.78, 44.1, 17.2 and 33.2% respectively. Based on the present investigation, the presence of nano-alumina particles contribute more on crystallite size variation and dispersion strengthening. Therefore, the incorporation of nano-alumina on Cu–10Zn matrix will enhance the mechanical properties.

#### 4 Conclusions

Bulk nanostructured novel (Cu–10Zn)-Al<sub>2</sub>O<sub>3</sub> nanocomposites were successfully manufactured and investigated by mechanical alloying and hot vacuum pressing. TEM microstructure explained the average crystallite size of Cu–

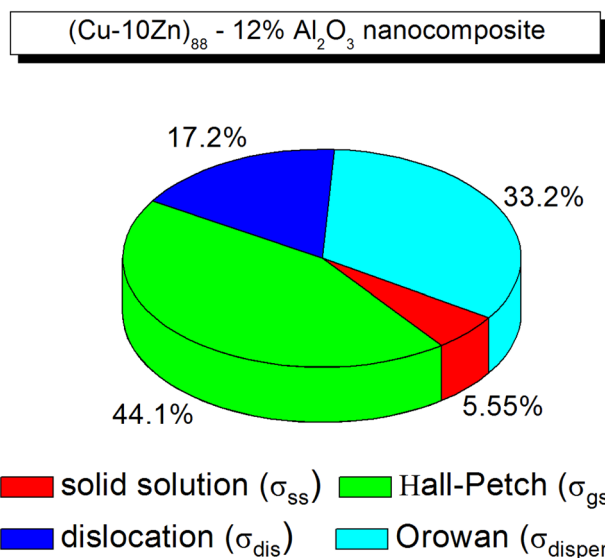


Fig. 7 Contribution of various strengthening mechanisms on total strength for (Cu–10Zn)<sub>88</sub>–12 wt% Al<sub>2</sub>O<sub>3</sub> nanocomposites

Zn of  $\alpha$ -brass matrix, which were 280 nm, 230 nm, 184 nm, 152 nm and 122 nm for 0, 3, 6, 9 and 12 wt% Al<sub>2</sub>O<sub>3</sub> reinforced nanocomposites respectively after sintering. These results revealed that the incorporation of nano-alumina particles pinned the grain growth considerably due to Zener pinning action or pressure in crystallite boundaries. The measured bulk density of all sintered samples exhibited more than 91% on theoretical density. Based on simple compression results, calculation of work hardening rate and strain hardening exponent values, (Cu–10Zn)<sub>94</sub>–6Al<sub>2</sub>O<sub>3</sub> nanocomposite produced more ductility when compared to other samples investigated here. It exhibited considerable strength (810 MPa), more amount of work hardening rate and it had shown the strain hardening exponent of 0.34. This might be attributed to the achievement of good interfacial bonding between nano-alumina particles and Cu–10Zn matrix which might have led to effective load transfer between them (Fig. 2). Though, the higher reinforced nanocomposites (12%) exhibited more ultimate compressive strength, it produced poor ductility due to more intergranular and transgranular brittle fractures which were evidenced by SEM fractography. Further, grain size strengthening and Orowan strengthening contributed to the total strength when compared to other strengthening mechanisms of solid solution and dislocation strengthening.

#### References

1. Meyers M A, Mishra A, Benson D J, *Prog Mater Sci* **51** (2006) 427.

2. Balogh L, Ungar T, Zhao Y, Zhu YT, Horita Z and Xu C, *Acta Mater* **56** (2008) 809
3. Zhao Y H, Liao X Z, Horita Z, Langdon T G and Zhu Y T, *Mater Sci Eng A* **493** (1-2) (2008) 123
4. Haiming Wen, Troy D. Topping, Dieter Isheim, David N. Seidman and Lavernia E J, *Acta Materialia* **61** (2013) 2769
5. Li X C, Yang Y and Cheng X D, *J. Mater. Sci.* **39** (2004) 3211
6. Sivasankaran S, Sivaprasad K, Narayanasamy R and Satyanarayana P V, *Mater. Charact* **62** (2011) 661
7. Canakci A and Varol T, *Powder Technol.* **268** (2014) 72
8. Razavi Hesabi Z, Simchi A, Seyed Reihani S M, *Mater. Sci. Eng. A* **428** (2006) 159
9. Sivasankaran S, Sivaprasad K, Narayanasamy R and Vijay Kumar Iyer, *J. Alloys Compd* **491** (2010) 712
10. Tang F, Hagiwara M and Schoenung J M, *Scr. Mater.* **53** (2005) 619
11. Sivasankaran S, Sivaprasad K, Narayanasamy R and Saravanan M, *Int. J. Adv. Manuf. Technol.* **78** (1) (2015) 385
12. Cheng-jin H U, Hong-ge Y A N, Ji-hua C H E N and Bin S U, *Trans. Nonferrous Met. Soc. China* **26**(5) (2016) 1259
13. Shang C, Axinte E, Sun J, Li X, Li P, Du J, Qiao P and Wang Y, *Mater. Des.* **117** (2017) 193.
14. Sivasankaran S, Sivaprasad K, Narayanasamy R and Vijay Kumar Iyer, *J. Alloys Compd* **507** (2010) 236
15. Srivastav A K, Panindre A M and Murty B S, *Trans Indian Inst Met* **66**(4) (2013) 409
16. Mehrizi M Z, Shamanian M and Saidi A, *Trans Indian Inst Met* **67**(5) (2014) 67(5) 709
17. Ramkumar K R, Ilangovan S, Sivasankaran S and Alaboodi A S, *J. Alloys Compd* **688** (2016) 518
18. Liu G, Zhang G J, Jiang F, Ding X D, Sun Y J, Sun J and Ma E, *Nat. Mater.* **12** (2013) 344
19. Zhao Y H, Liao X Z, Cheng S, Ma E and Zhu Y T, *Adv. Mater.* **18** (2006) 2280
20. W.D. Callister Jr., *Materials Science and Engineering: An Introduction*, seventh ed., John Wiley and Sons, New York, 2007.
21. Humphreys F J, *Acta Mater.* **45** (1997) 5031
22. Kang J L, Nash P, Li J J, Shi C S and Zhao N Q, *Int. J. Nanotechnol* **20** (2009) 1.
23. Cha S I, Kim K T, Arshad S N, Mo C B and Hong S H, *Adv. Mater.* **17** (2005) 1377
24. Degarmo, E. Paul; Black, J T.; Kohser, Ronald A. (2003), *Materials and Processes in Manufacturing* (9th ed.), Wiley, ISBN 0-471-65653-4
25. Lu L, Wang L B, Ding B Z and Lu K, *J. Mater. Res.* **15** (2000) 270
26. Dixit M, Mishra R S and Sankaran K S, *Mater. Sci. Eng., A* **478** (2008) 163
27. Li M, Zhai H, Huang Z, Liu X, Zhou Y, Li S and Li C, *J. Alloys Compd* **628** (2015) 186
28. Cheng, Y. T and Cheng, C. M. (1998), Scaling approach to conical indentation in elastic-plastic solids with work hardening, *J. Appl. Phys.* **84**(3) (1998) 1284
29. Shanmugasundaram, T., Heilmaier M, Murty B S and Sarma V S, *Metall. Mater. Trans. A.*, **40**(12) (2009) 2798
30. Hsu C J, Chang C Y, Kao P W, Ho N J and Chang C P, *Acta Mater.* **54** (2006) 5241